Converter Model for Representing Converter Interfaced Generation in Large Scale Grid Simulations

Deepak Ramasubramanian, *Student Member, IEEE*, Ziwei Yu, Rajapandian Ayyanar, *Senior Member, IEEE*, Vijay Vittal, *Fellow, IEEE*, and John Undrill, *Fellow, IEEE*

***Abstract*—This paper addresses the positive sequence modeling of converter-based sources in commercial transient stability analysis software. A simple and computationally economical model of the converter has been developed while ensuring a reliable representation of the detailed converter behavior. This model has been implemented as a user defined model in commercial positive sequence software such as PSLF. The behavior of the proposed model in positive sequence has the same form as the behavior obtained from detailed point on wave simulation. Tests have been carried out on a three-generator nine-bus equivalent system and the 18,205 bus Western Electricity Coordinating Council system to assess the impact and performance of the converters. The behavior of these converter interfaced generation sources for various system contingencies has been investigated.**

***Index Terms*—Converter-based source, droop control, PLECS, positive sequence, PSLF, WECC system.**

I. Introduction

In the past few years, there has been an increase in the number of grid connected converter interfaced generation (CIG) sources to meet renewable portfolio standards. The bulk power system presently has a small penetration of CIG. However as the penetration increases, it is important to be able to study the impact of such fast acting sources on the stability of the system. Since it is not possible to carry out a detailed microsecond time step simulation of large power systems with CIG, dynamic models have to be developed to represent the behavior of the converter accurately in positive sequence transient stability simulations.

There are several articles in literature which address dynamic performance of power systems with CIG. Tackling a hybrid microgrid, [1] explores the mechanism of automatic frequency and voltage control in an islanded microgrid while highlighting the derated operation of the renewable energy source to bring about a reserve margin. With an increased penetration of CIG in the transmission system, it would be worthwhile to have these sources contribute to the frequency recovery following large disturbances. Reference [2] presents a few of the key issues that surround this issue. The authors mention the necessity of designing primary and secondary frequency response control loops which would act in the presence of minimal storage devices. Additionally, concerns have been raised about the lack of accurate dynamic models to represent these sources. Other papers, [3]–[6], have tackled the issue of wind turbine generators participating in system frequency regulation. These papers discuss a variety of control mechanisms and strategies specific to wind turbines. Their testing and validation have however been performed only on small systems.

The replacement of conventional synchronous machines by CIG necessitates the transfer of primary and secondary frequency control methodologies to CIG. Applying droop control to converters within a microgrid for primary frequency regulation has been discussed in [7]–[13] while the use of energy storage devices to support frequency regulation and analysis on the best return of investment methodology has been discussed in [14]–[17].

With the consideration of a large system for analysis, namely the Western Electricity Coordinating Council (WECC) system, [18] examined the impact of CIG on the small signal and transient stability. A portion of the conventional generation was replaced to include these sources. However, they were added only to those parts of the system that contained relatively large amounts of conventional generation. It has also been assumed that the reactive power support decreases with increase in CIG as most of the sources are rooftop PV which are not allowed to regulate voltage as per the existing grid code. The utility scale PV sources however provide reactive power support. The analysis has been carried out with a maximum renewable resource penetration of 20%. Further, the PV sources were assumed to operate in a constant power mode without the presence of droop control.

This paper describes a positive sequence converter model developed for the purpose of coupling CIG into the standard production version of a large scale grid simulation. While the modeling of converters at the point-on-wave level and the "average voltage" level is well established [19], difficulties arise in coupling many established converter models into the network modeling of large scale grid simulation programs.

The positive sequence converter model for a CIG developed in this paper makes use of and demonstrates the effect of the fast maneuvering capability of a CIG on the power system. When connected to the network through converters, sources like solar, wind and batteries can very quickly provide frequency and voltage support upon the occurrence of a disturbance.

Manuscript received December 7, 2015; revised February 15, 2016; accepted April 3, 2016. Date of publication April 6, 2016; date of current version December 20, 2016. This work was supported by the National Science Foundation under the Grant EEC-9908690 at the Power System Engineering Research Center. Paper no. TPWRS-01752-2015.

The authors are with the School of Electrical, Computer, and Energy Engineering, Arizona State University, Tempe, AZ 85281 USA (e-mail: dramasu1@asu.edu; ziweiyu@asu.edu; rayyanar@asu.edu; vijay.vittal@asu.edu; jundrill@q.com).

Color versions of one or more of the figures in this paper are available online at http://ieeexplore.ieee.org.

Digital Object Identifier 10.1109/TPWRS.2016.2551223

The convergence properties of the network solution in conjunction with the boundary conditions imposed by loads and converter coupled devices is strongly influenced by the form in which the boundary condition is expressed [20]–[22]. The models described in [23], [24] (henceforth referred to as boundary current representation) form the converter boundary conditions as a nonlinear algebraic relationship between complex power and the current and voltage phasors at the point of connection. In contrast, the model described in this paper is interfaced with the network by a Thévenin voltage source. This approach has given good convergence of the network solutions in our simulations. Additionally, it will be shown that the boundary current representation is unable to capture the near instantaneous response possible from controlled converters. Many research efforts are now tackling the task of improving the representation of CIG in positive sequence time domain simulations [25].

Converters, in practice, are voltage sources which generate an ac side voltage by manipulating the switching of the solid state switches. In the proposed Thévenin representation, the current injected into the network is now due to the generated voltage and the terminal voltage on the network side of the coupling inductor. It will be shown that this explicit representation of the coupling inductor directly impacts the behavior of the converter at the instant of disturbance.

Applications of this proposed model in simulations of the WECC system at the 18,000 bus level, to illustrate its performance, are shown in this paper. In addition, simulations conducted with this proposed controlled voltage source representation are shown in comparison with point-on-wave simulations to provide a calibration. The point-on-wave simulations were made with the PLECS [26] software package using established modeling of internal aspects of converters.

It must be emphasized here that the ***focus*** of this paper is on the development of a positive sequence model to represent the converter in simulation studies. The control architecture used to generate the commands for the converter is a simple and generic control structure since a wide range of control techniques exist in practice which vary with the type of energy source and the manufacturer of the associated equipment. Thus, in order to avoid resemblance with any particular type of control structure, a ***simple generic control*** has been used to achieve the required goal of generating the commands for the proposed converter model.

The remainder of the paper is organized as follows: Section II describes the development of the converter model along with its associated control architecture. Section III shows the behavior of the developed model in commercial software on an all CIG system and a large power network. Section IV summarizes the need for the controlled voltage source representation while Section V concludes the paper.

II. Converter Model

A. Proposed Converter Model

In this paper, a controlled voltage source representation of the converter is proposed to incorporate the effect of the converter coupling inductance. This representation captures the near instantaneous response that can be achieved from converter interfaced sources.

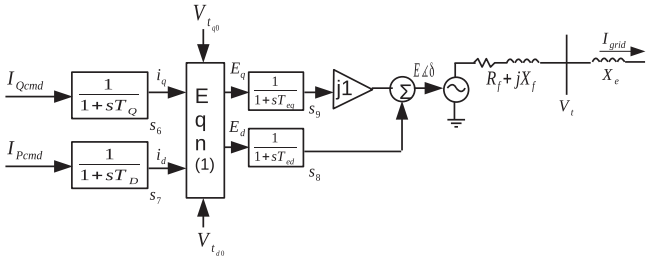

Fig. 1. Controlled voltage source converter representation for positive sequence simulation.

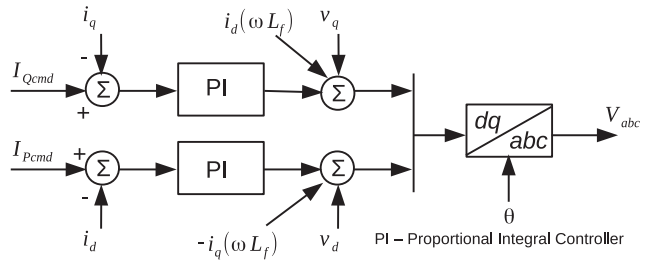

Fig. 2. Inner current control loop in PLECS to synthesize reference voltage wave.

As the converter is practically a controlled ac voltage source with a voltage source on the dc side, the converter is modeled as a Thévenin voltage source described by Fig. 1 and (1)

$$\begin{aligned} E_d &= V_{t_{d0}} + i_d R_f - i_q X_f \\ E_q &= V_{t_{q0}} + i_q R_f + i_d X_f . \end{aligned} \tag{1}$$

The impedance $R_f + jX_f$ represents the coupling inductance which can be either a filter inductor or a transformer while E and δ represent the magnitude and angle of the developed converter voltage. $V_{t_{d0}}$ and $V_{t_{q0}}$ represent the *dq* axis components of the terminal voltage V_t. The current commands, $I_{Q_{\mathrm{cmd}}}$ and $I_{P_{\mathrm{cmd}}}$, represent the real and reactive current commands provided by the outer loop control. The time constants T_Q and T_D represent the effect of the inner current control loop of the converter control structure.

B. PLECS Model for Calibration

The positive sequence model was calibrated by comparing its results with results from a point on wave simulation program, PLECS. In the PLECS simulation, the pulse width modulated voltage source was represented by three amplitude and phase modulated sinusoidal voltage sources connected phase to neutral. This representation of the converter can be referred to as an average model [19]. The inner current control loop uses the generated current commands as shown in Fig. 2 to synthesize the reference voltage wave to be developed by the converter. While the fast inner current control loops are required in the electromagnetic transient simulation, this detail of modeling the voltage source converter and its control is however not suitable for the transient stability simulation of large networks as it would require a smaller simulation time step to accurately capture the inner loop behavior and this would considerably increase the time duration of simulation.

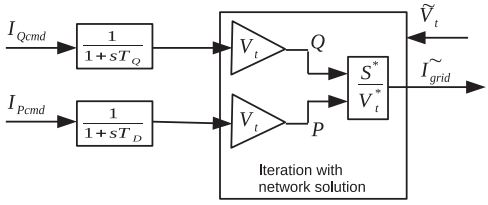

Fig. 3. Boundary current converter representation for positive sequence simulation.

Due to the effect of grid impedance on the operation of the inner current control loop [27], a wide variety of inner current control loops are used in practical inverters with the common characteristic of response times that are very fast in relation to the bandwidth proposed for grid level controls. Accordingly, for the positive sequence grid level model used in this paper, simple time constants represented as T_D and T_Q with a value of 10 ms each represent the behavior of the inner control loops. This is a conservative estimate as in practice, these inner control loops may have a quicker response time. The time constants $T_{\rm ed}$ and $T_{\rm eq}$ also have a conservative value of 10 ms each and represent the delay in the pulse width modulation/switching process. Again, in reality, this value could be lower than 10 ms.

C. The Converter Interface

The converter model described by [23], [24] uses a boundary current interface between the converter model and the network as shown in Fig. 3. It is shown in the next section that this representation of the converter does not depict the near instantaneous response that can be achieved from a CIG. With a projected increase in CIG penetration in large systems, the ability of the CIG to provide a near instantaneous response to a disturbance can prove beneficial to the system and the positive sequence simulation model should be able to capture this feature.

The converter model proposed in this paper in Section II-A is interfaced with the network solution by a Thévenin voltage source which is a simple function of the state variables of the model and has a constant value from one iteration of the network solution to the next. This form of interface avoids the numerical convergence issues that can arise [20]–[22] when the model establishes a boundary condition based on the network solution.

D. Generic Control Structure

In order to generate the current commands $I_{Q\rm cmd}$ and $I_{P\rm cmd}$ a generic control structure as shown in Fig. 4 has been used. Due to the presence of a wide variety of proprietary vendor specific control structures, a simple generic control structure has been used in order to avoid conflict with any particular type of control structure.

The effective real power order [see Fig. 4(b)] is a combination of the power setpoint and the active power droop coefficient while the reactive power order [see Fig. 4(a)] is obtained from the voltage error along with a reactive power droop. The QV droop is instrumental in obtaining a stable operation between converters when multiple converters are connected to the same bus. The active power droop coefficient is denoted as R_p and the reactive power droop coefficient is denoted as R_q. The equations describing the behavior of the controller are given by (2) to (11)

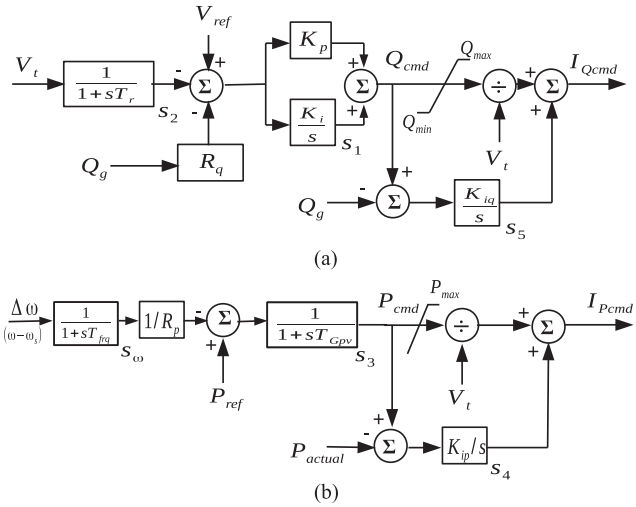

Fig. 4. Converter control model. (a) Reactive power controller. (b) Real power controller.

$$\frac{ds_1}{dt} = K_i\left[V_{\rm ref} - s_2 - R_q Q_g\right] \tag{2}$$

$$\frac{ds_2}{dt} = (1/T_r) * \left[V_t - s_2\right] \tag{3}$$

$$\frac{ds_\omega}{dt} = (1/T_{\rm frq}) * \left[\Delta\omega - s_\omega\right] \tag{4}$$

$$\frac{ds_3}{dt} = (1/T_{\rm Gpv}) * \left[P_{\rm ref} - (s_\omega/R_p) - s_3\right] \tag{5}$$

$$P_{\rm cmd} = s_3 \tag{6}$$

$$\frac{ds_4}{dt} = K_{\rm ip}\left[P_{\rm cmd} - P_{\rm actual}\right] \tag{7}$$

$$\frac{ds_5}{dt} = K_{\rm iq}\left[Q_{\rm cmd} - Q_{\rm actual}\right] \tag{8}$$

$$Q_{\rm cmd} = s_1 + K_p\left[V_{\rm ref} - s_2 - R_q Q_g\right] \tag{9}$$

$$I_{\rm Qcmd} = Q_{\rm cmd}/V_t + s_5 \tag{10}$$

$$I_{\rm Pcmd} = P_{\rm cmd}/V_t + s_4. \tag{11}$$

Limits have been imposed on the maximum active and reactive power and minimum reactive power deliverable. The methodology behind obtaining a numerical value for the limits has been described in the Appendix.

The next section describes the results of the implementation of the converter model shown in Fig. 1 on a three machine nine bus equivalent system and the 18,205 bus WECC system.

III. Simulation and Results

A. Justification of Value of Inner Current Loop Time Constants

To justify the use of a 10 ms time constant to represent the inner control loop (T_D and T_Q), a simple test network was set up in PLECS with a 247 MVA converter connected through a coupling reactor of 0.06 p.u., a step up transformer of

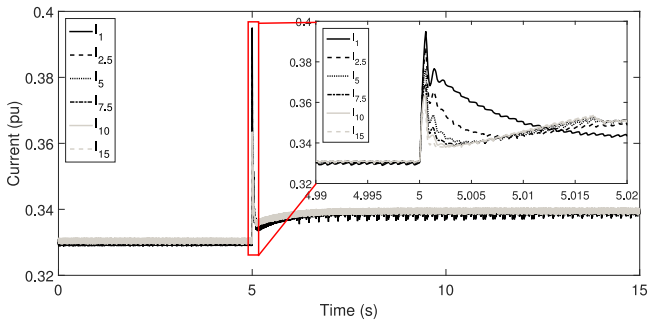

Fig. 5. Converter current output for 30 MW load increase with different PI controller gains.

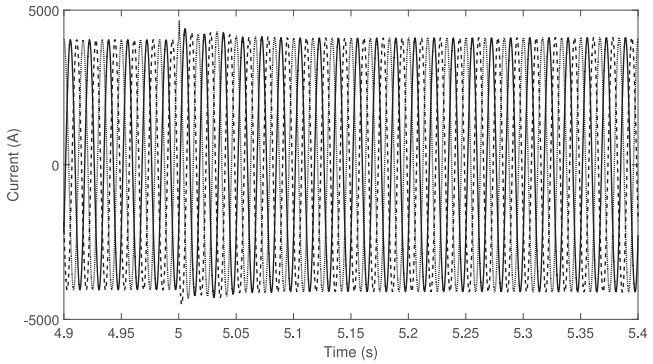

Fig. 6. Three phase converter current output for 30 MW load increase with proportional gain I_1.

0.05 p.u. and a short line of (0.017 + j0.092) p.u. to an infinite bus. A local load of 90 MW and 30 MVAR was also present at the high voltage side of the transformer. At $t = 5$ s, the local load was increased by 30 MW. The output current magnitude of the converter for different values of proportional gain of the PI controller of Fig. 2 is as shown in Fig. 5. The subscript indicates the factor by which the original gain was multiplied. The active power setpoint of the converter was at 80 MW. From the figure it can be seen that the magnitude of the near instantaneous response of the converter is controllable by adjusting the proportional gain of the PI controller. It can also be seen that irrespective of the value of the proportional gain, the response trend is similar 10 ms after the occurrence of the disturbance. The near instantaneous rise and subsequent settling of the converter current can also be observed from the plots of the three phase currents as seen in Fig. 6. These figures showcase the fast maneuvering capability of a CIG.

While conducting positive sequence simulations, the standard time step of integration is taken as a quarter cycle of a 60 Hz sine wave. With this time step, it is impossible to accurately depict the same response as obtained in Fig. 5. However, for the purpose of studying the behavior of the converter in a large system, it is sufficient for the response from the positive sequence software to have the same form as that obtained from the PLECS response within the bandwidth of the grid simulation. This validates the usage of the 10 ms time constant to represent the inner control loop. Further, for calibration and comparison, the proportional gain in PLECS was suitably chosen as will be shown in the following section.

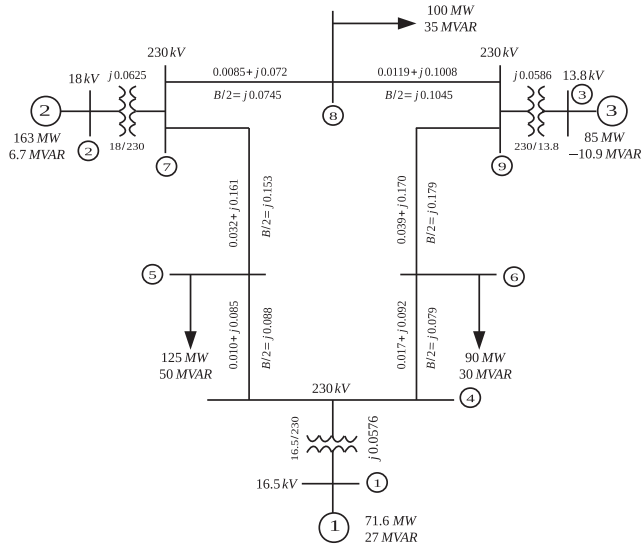

Fig. 7. Three machine nine bus equivalent system.

The proposed positive sequence converter model (see Section II-A) and the boundary current converter model (see Section II-C) were implemented with the "user written model" feature of the large scale grid simulation program PSLF [28] for further comparison of performance. A user written model in PSLF is known as an "epcgen" model wherein the mathematical model of the generation source is developed using PSLF's EPCL programming language.

B. Small Scale System-Validation of Results

A three machine nine bus equivalent system [29] shown in Fig. 7 was used to validate the performance of the developed converter model along with its associated control in PSLF. The behavior of this model to an increase in load was compared with its behavior in PLECS for the same disturbance. Simultaneously, the behavior of the proposed controlled voltage source converter model was also compared with the existing boundary current representation converter model. With the loads treated as constant admittance, the load at bus 6 was increased by 10 MW at $t = 5$ s. The proportional and integral gains of the PI controller in the reactive power loop were taken as 4.0 and 20.0 respectively while the integral gains K_{ip} and K_{iq} were each 10.0. The value of R_p was taken to be 0.05 p.u. on a 100 MVA system base while R_q was taken as 0.0. The value of R_f was taken to be 0.0025 p.u. while X_f was taken to be 0.06 p.u. on the converter MVA base. In this paper, the value of X_f was chosen to restrict the current ripple to a maximum of 5% and limit the THD in voltage to 3%.

In the first scenario, only the machine at bus 1 was replaced with a converter while the machines at buses 2 and 3 were retained as synchronous machines with associated governors and static exciter models. Fig. 8 shows the active power output of the converter at bus 1. The PLECS response has been compared with both the voltage and boundary current representation of the converter in positive sequence. The inset shows the response of

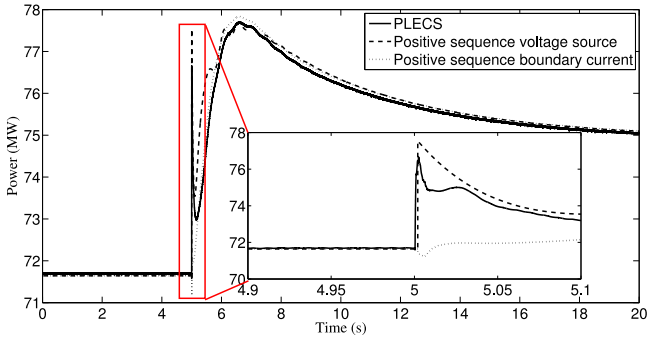

Fig. 8. Comparison of the active power output of converter at bus 1 between PLECS and the "epcgen" model in PSLF with synchronous machines at buses 2 and 3.

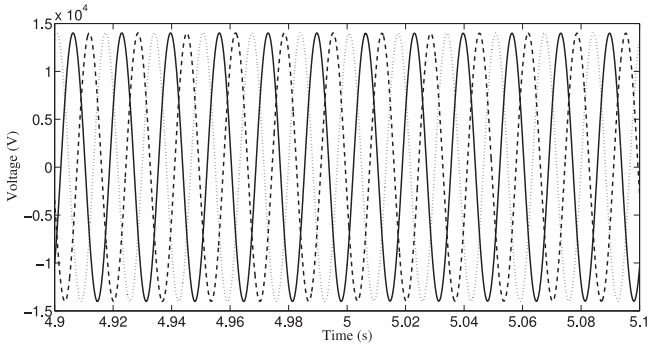

Fig. 9. Phase voltage waveforms at the converter terminal from PLECS.

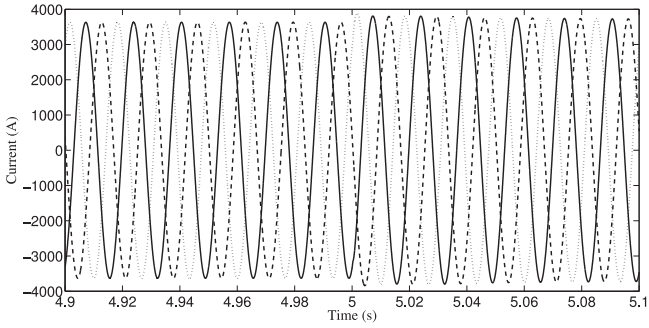

Fig. 10. Line current waveforms at the converter terminal from PLECS.

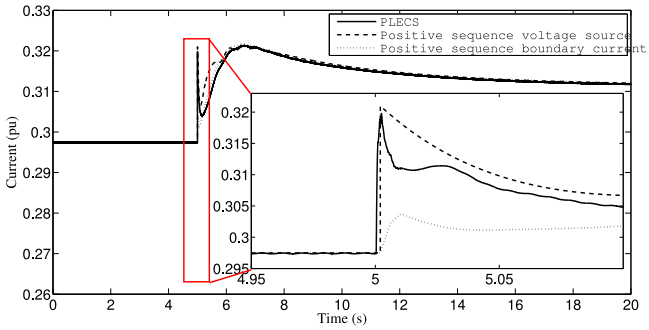

Fig. 11. Comparison of current output of converter at bus 1 between PLECS and the "epcgen" model in PSLF with synchronous machines at buses 2 and 3.

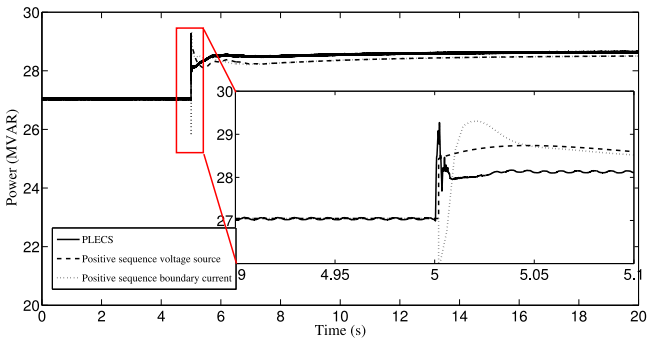

Fig. 12. Comparison of reactive power output of converter at bus 1 between PLECS and the "epcgen" model in PSLF with synchronous machines at buses 2 and 3.

the models at the instant of disturbance. It can be seen that both the proposed controlled voltage source representation of the converter model and the PLECS response capture the near instantaneous response achievable by the converter while the boundary current representation is unable to do so. The difference in the peak value between the voltage source representation response and the PLECS response can be attributed to the fact that the time step of simulation is much smaller in PLECS which allows for the change in the internally generated converter voltage upon recognition of the disturbance. In the positive sequence simulation however, at the instant of disturbance, the internally generated converter voltage is constant while the terminal voltage changes.

The instantaneous three phase voltage and current waves at the converter terminals are as shown in Figs. 9 and 10 respectively. These figures show that there is a negligible change in the terminal voltage while the converter current rises near instantaneously to meet the demand. The magnitude of the converter current output from PLECS is compared with the positive sequence simulations as shown in Fig. 11. It can be seen that the near instantaneous response achievable by the converter is captured by voltage source representation of the converter. The reactive power response is shown in Fig. 12. It can be immediately observed from this figure that the voltage source representation response is the more acceptable positive sequence phasor approximation to the point on wave simulation. From the inset of the figure it can be seen that the reactive power trajectory of the boundary current simulation is evidently inconsistent with the result from the PLECS simulation. The trajectory produced by the voltage source positive sequence model, while not reproducing the slight oscillatory component of the electromagnetic response, is consistent with the PLECS simulation in the direction of its initial change. This difference in the response at the instant of disturbance justifies the use of the voltage source representation as the model of choice for the simulation of large systems. Due to the absence of any connection to ground at the terminal bus of the converter in the positive sequence boundary current representation, the network solution results in an instantaneous large voltage dip at the instant of disturbance. This results in the initial change of reactive power in the direction opposite to the PLECS simulation.

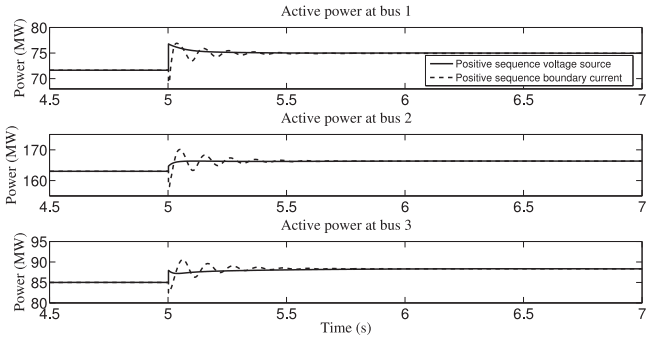

Fig. 13. Active power output of the converters for an all CIG system.

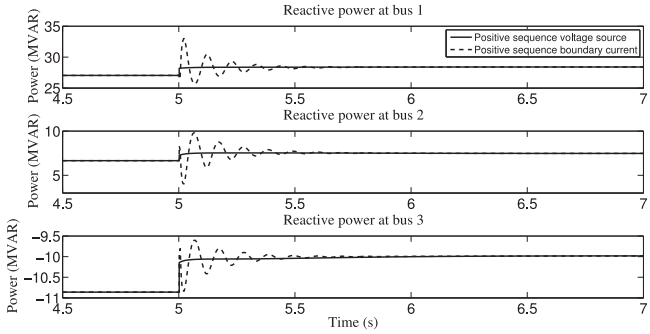

Fig. 14. Reactive power output of the converters for an all CIG system.

In order to examine an all CIG system, the machines at buses 2 and 3 were also replaced with both forms of the positive sequence converter model. The instantaneous rise in the active power of the voltage source representation can be calculated on the same lines as the distribution of impact calculation for synchronous machines.

Based on the electrical distance between the internal voltage source of the converter and the disturbance point, the instantaneous response of a converter at bus *i* for an impact at bus *k* can be obtained as

$$P_{i\Delta}(0^+) = \left(P_{\text{sik}} / \sum_{j=1}^{n} P_{\text{sjk}} \right) P_{L\Delta}(0^+) \quad i = 1, 2, \ldots, n \qquad (12)$$

where

$$P_{\text{sik}} = V_i V_k \left(B_{\text{ik}} \cos \delta_{\text{ik0}} - G_{\text{ik}} \sin \delta_{\text{ik0}} \right) \qquad (13)$$

and $P_{L\Delta}(0^+)$ is the load impact at bus *k*. The entire derivation of (12) is available in [29].

For the same load increase of 10 MW at bus 6, the active power output from the converters is as shown in Fig. 13 while Fig. 14 shows the reactive power output. With the final steady state values being almost the same, the behavior of the models at the instant of disturbance becomes the deciding factor. It can be seen that in an all CIG system too, the boundary current representation response instantaneously moves in a direction opposite to what would be expected while the response from the voltage source representation is as expected and it conforms to (12). It has thus been established that the voltage source representation of the converter is the more appropriate representation in positive sequence phasor simulations of large systems.

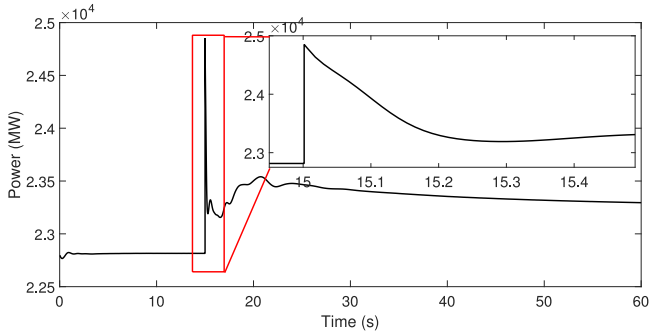

Fig. 15. Active power generation in the Arizona area due to trip of two Palo Verde units.

C. Large Scale System-Economy of Computation

To ensure that this model is practical in a large scale system, the WECC 2012 system has been used. While at this stage it is not important to test the performance of this model relative to the conventional representation of machines, it is important to test the robustness and numerical behavior of the model when a large number of converters are present in the system. This system has 18,205 buses, 13,670 lines and 2592 generators. The total generation is 176 GW while the total load is 169 GW. To obtain a sizable presence of converters, all the generators in the Arizona and Southern California area (528 units) were replaced with converters represented by the proposed voltage source representation (see Section II-A). This accounted for 24.3% of the total system generation with 25.6 GW in Arizona and 17 GW in Southern California. A similar study has been reported in [30] wherein the penetration over the entire system was taken to be as high as 53%. The distribution of such sources was however spread out across the entire system and not concentrated in one region as examined in this paper. Further, in [30] the concentrating solar power plants were modeled as synchronous machines while the wind and the utility scale photovoltaic plants were modeled as full four quadrant converters represented as a boundary current representation.

At $t = 15$ s, two of the Palo Verde units were tripped resulting in a generation outage of 2755 MW. Fig. 15 shows the power output from the remaining sources in the Arizona area when all machines were replaced with converters. For each converter, the value of the droop coefficient R_p was taken to be the same as that used by the governor of the synchronous machine it replaced while R_q was taken to be 0.05 p.u. on the converter MVA base. The reactive power PI controller gains of all converters were set to $K_p = 1.0$ and $K_i = 5.0$ while the integral gains K_{ip} and K_{iq} had a value of 10.0 each. The value of R_f and X_f were taken as 0.004 and 0.05 p.u. on the converter MVA base. It can be observed from the figure that the simulation is numerically stable and the response is consistent with expectations. The effect on the adjacent area of Southern California is shown in Fig. 16. The effect of this generation outage on the flow of power between these two areas is as shown in Fig. 17 while the system frequency plot is shown in Fig. 18. The fast action of the converters can be observed from the frequency response when compared to the response with all units represented as conventional synchronous machines. The presence of voltage

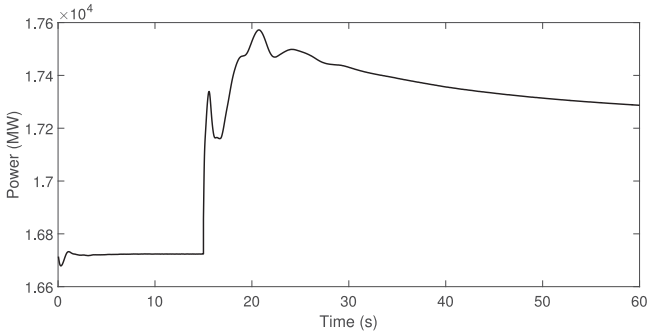

Fig. 16. Total generation in Southern California area due to trip of two Palo Verde units.

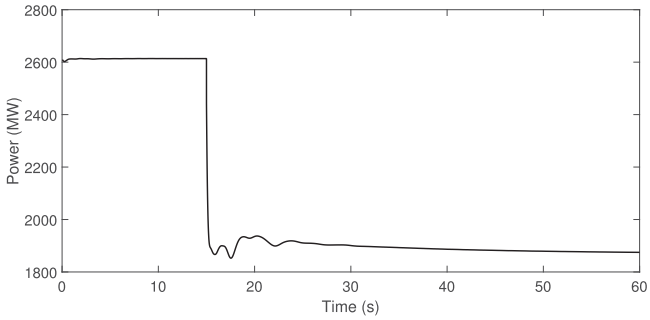

Fig. 17. Active power flow from Arizona to Southern California due to trip of two Palo Verde units.

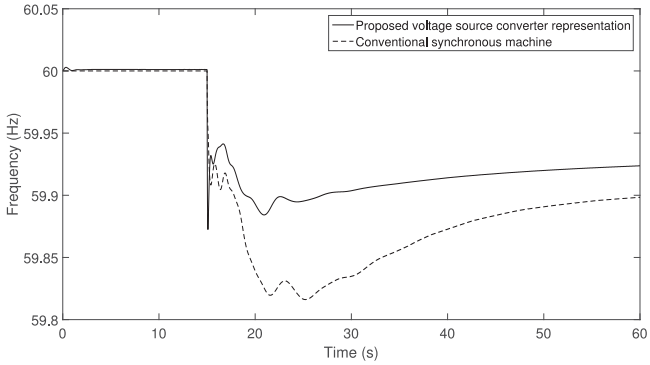

Fig. 18. System frequency due to trip of two Palo Verde units.

control on all CIG units results in a different steady state loading thus resulting in a different steady state frequency.

In terms of computation time, PSLF took 7:04 min to run this 60 s simulation with the first 20 s of simulation taking 1:52 min. In comparison to this, when all machines were represented as conventional generators, the same 60 s simulation took 6:41 min with the first 20 s of simulation being completed in 1:39 min. Both simulations were run on a machine with an i7 processor and 16.0 GB of RAM with a simulation time step of 0.0041 s.

The behavior of the system following the occurrence of a line fault was tested next. A three phase fault was applied on a tie line between Arizona and Southern California at $t = 15$ s. Subsequently, at $t = 15.05$ s, the breakers at both ends of the line were opened. The initial flow on the line was 1408.6 MW

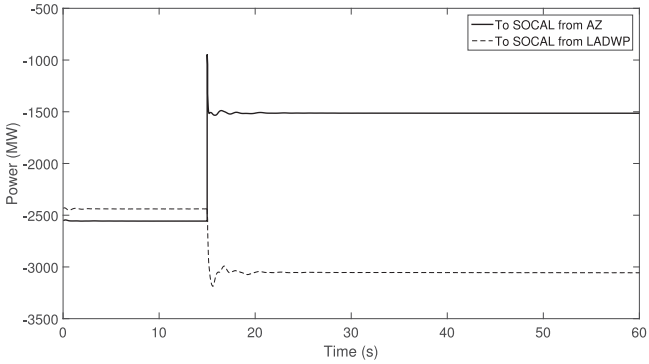

Fig. 19. Active power flow to Southern California from Arizona and LADWP with the opening of a tie line between Arizona and Southern California following a line fault.

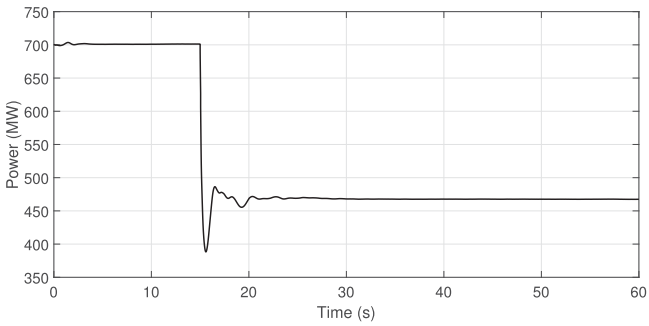

Fig. 20. Active power flow from Southern California to San Diego with the opening of a tie line between Arizona and Southern California following a line fault.

and 134.4 MVAR from the Arizona side. Figs. 19 and 20 show the changes in the power transfer between Southern California and the areas of Arizona, Los Angeles Department of Water and Power (LADWP) and San Diego. Negative values indicate that the power flow is into Southern California while positive values indicate power flow out of the region. The opening of the line causes a reduction in flow between Arizona and Southern California as expected.

It should be noted that only the voltage source representation of the converter was able to function reliably following the fault. The boundary current representation of the converters resulted in frequent non convergence issues with regard to the network solution following the occurrence of the fault as it was unable to represent the near instantaneous response available from CIG to a disturbance.

The third test carried out on the WECC system was applying a bus fault for 0.1 s at $t = 15$ s near the Four Corners generation plant in the Arizona area. The active power and terminal voltage of one of the units is as shown in Figs. 21 and 22. From the active power plot the familiar damped rotor angle oscillations can be observed from the output of the synchronous machine. In addition, it can also be seen that a large electronic source brings about a highly damped response. However, the voltage dip in the converter response is smaller than that of the corresponding synchronous machine. The value of the coupling inductor X_f along with the absence of a sub-transient capability influences the magnitude of this dip in voltage. The magnitude of the

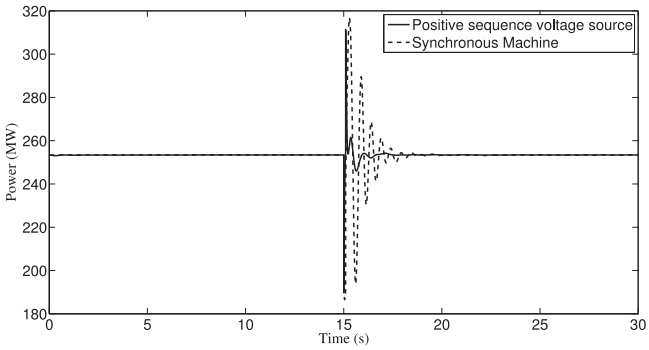

Fig. 21. Active power output of a unit at Four Corners for a bus fault close to the unit.

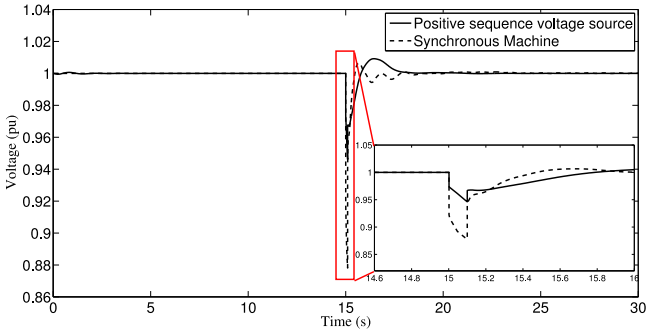

Fig. 22. Terminal voltage of a unit at Four Corners for a bus fault close to the unit.

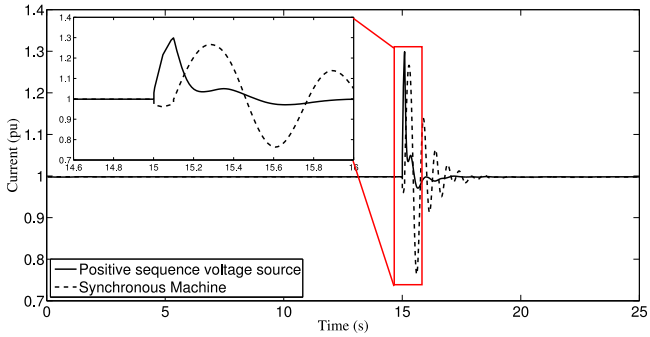

Fig. 23. Magnitude of converter current for a voltage source representation of the converter for a bus fault close to the unit.

converter current for the voltage source representation is as shown in Fig. 23. The current is well within its short time current rating of 1.7 p.u. It has also been observed that for few other significant bus faults, the network solution diverges when the boundary current representation is used.

IV. Note on Boundary Current Representation

In order to study the effect of a large penetration of CIG in power systems, it is very important that the computer simulation models have a reliable representation of the converter. It has been shown in this paper that the boundary current representation is not a suitable representation due to the following reasons:

1) It is unable to capture the near instantaneous response that can be achieved by a CIG following a disturbance.

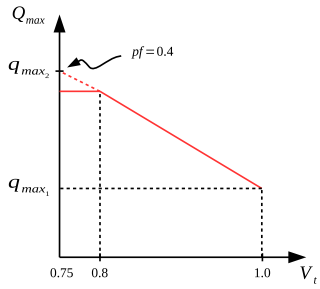

Fig. 24. Variation of Q_{limit} with V_t.

2) The initial change of the reactive power trajectory does not conform with the expected change.
3) The absence of the coupling inductor results in a larger voltage dip as compared to the voltage source representation and the PLECS response.
4) The network solution fails to converge for simulations of certain contingencies in large systems.

In each case mentioned above, the voltage source representation is consistent with the properties of these devices and is thus a more appropriate approximation of the electromagnetic transient model for positive sequence simulations.

V. Conclusion

This paper has addressed the issue of development of practical dynamic models to represent the behavior of converter based sources in positive sequence commercial software. A simple control structure has been used to take care of both active and reactive power control in a straightforward manner and a voltage source representation of the converter has been proposed. The development of this converter model has been calibrated by comparison to a detailed electromagnetic transient model. It has also been shown that CIG modeled in this manner have a significant effect on the system response to a disturbance and these models have been shown to behave in a satisfactory manner in a large realistic system. However, as the location of connection of the CIG to the network and its energy source play a role in its response, future research work is required to exactly determine the value of the time constants in the positive sequence model to exactly match the response from the electromagnetic transient program.

Appendix

In choosing the limits for reactive and active power, it has been assumed that the converter can withstand an instantaneous MVA of 1.7 times its rating. Further, it has been assumed that at a terminal voltage level of 0.75 p.u., the minimum operable power factor is 0.4. As the voltage dips, the limits on the converter control will change to allow for more reactive power to be delivered while curtailing the active power delivered to meet the MVA rating. Though a terminal voltage of 0.75 p.u. has been chosen as the minimum voltage, the maximum deliverable reactive power is maintained constant for voltages below 0.8 p.u. as shown in Fig. 24. The value of q_{max_1} is taken from the power flow but is assumed to be the value of maximum re-

active power at a voltage level of 1.0 p.u. The value of $q_{\max_2}$ is obtained as given by (14)

$$q_{\max_2} = \sqrt{\frac{(1.7 * MVA)^2}{1 + \left(\frac{1}{\tan\cos^{-1} 0.4}\right)^2}}. \quad (14)$$

Therefore, at any voltage level V_t above 0.8 p.u., the value of $q_{\max}$ is obtained from Fig. 24 while $p_{\max}$ is obtained to maintain an MVA of $1.7 * \text{MVA}_{\text{rated}}$.

REFERENCES

[1] S. Mishra, D. Ramasubramanian, and P. Sekhar, "A seamless control methodology for a grid connected and isolated pv-diesel microgrid," *IEEE Trans. Power Syst.*, vol. 28, no. 4, pp. 4393–4404, Nov. 2013.

[2] H. Bevrani, A. Ghosh, and G. Ledwich, "Renewable energy sources and frequency regulation: survey and new perspectives," *IET Renew. Power Gener.*, vol. 4, no. 5, pp. 438–457, Sep. 2010.

[3] R. de Almeida and J. Peças Lopes, "Participation of doubly fed induction wind generators in system frequency regulation," *IEEE Trans. Power Syst.*, vol. 22, no. 3, pp. 944–950, Aug. 2007.

[4] I. Erlich and M. Wilch, "Primary frequency control by wind turbines," in *Proc. IEEE Power & Energy Soc. General Meeting*, Jul. 2010, pp. 1–8.

[5] J. F. Conroy and R. Watson, "Frequency response capability of full converter wind turbine generators in comparison to conventional generation," *IEEE Trans. Power Syst.*, vol. 23, no. 2, pp. 649–656, May 2008.

[6] A. Attya and T. Hartkopf, "Control and quantification of kinetic energy released by wind farms during power system frequency drops," *IET Renew. Power Gener.*, vol. 7, no. 3, pp. 210–224, May 2013.

[7] T. Vandoorn, B. Meersman, J. De Kooning, and L. Vandevelde, "Transition from islanded to grid-connected mode of microgrids with voltage-based droop control," *IEEE Trans. Power Syst.*, vol. 28, no. 3, pp. 2545–2553, Aug. 2013.

[8] K. Vidyanandan and N. Senroy, "Primary frequency regulation by deloaded wind turbines using variable droop," *IEEE Trans. Power Syst.*, vol. 28, no. 2, pp. 837–846, May 2013.

[9] R. Majumder, B. Chaudhuri, A. Ghosh, R. Majumder, G. Ledwich, and F. Zare, "Improvement of stability and load sharing in an autonomous microgrid using supplementary droop control loop," *IEEE Trans. Power Syst.*, vol. 25, no. 2, pp. 796–808, May 2010.

[10] Y. A.-R. I. Mohamed and E. El-Saadany, "Adaptive decentralized droop controller to preserve power sharing stability of paralleled inverters in distributed generation microgrids," *IEEE Trans. Power Electron.*, vol. 23, no. 6, pp. 2806–2816, Nov. 2008.

[11] E. Barklund, N. Pogaku, M. Prodanovic, C. Hernandez-Aramburo, and T. Green, "Energy management in autonomous microgrid using stability-constrained droop control of inverters," *IEEE Trans. Power Electron.*, vol. 23, no. 5, pp. 2346–2352, Sep. 2008.

[12] S. Ashabani and Y.-R. Mohamed, "General interface for power management of micro-grids using nonlinear cooperative droop control," *IEEE Trans. Power Syst.*, vol. 28, no. 3, pp. 2929–2941, Aug. 2013.

[13] G. Diaz, C. Gonzalez-Moran, J. Gomez-Aleixandre, and A. Diez, "Scheduling of droop coefficients for frequency and voltage regulation in isolated microgrids," *IEEE Trans. Power Syst.*, vol. 25, no. 1, pp. 489–496, Feb. 2010.

[14] H. Xin, Y. Liu, Z. Wang, D. Gan, and T. Yang, "A new frequency regulation strategy for photovoltaic systems without energy storage," *IEEE Trans. Sustain. Energy*, vol. 4, no. 4, pp. 985–993, Oct. 2013.

[15] W. Omran, M. Kazerani, and M. Salama, "Investigation of methods for reduction of power fluctuations generated from large grid-connected photovoltaic systems," *IEEE Trans. Energy Convers.*, vol. 26, no. 1, pp. 318–327, Mar. 2011.

[16] M. Datta, T. Senjyu, A. Yona, T. Funabashi, and C.-H. Kim, "A frequency-control approach by photovoltaic generator in a pv-diesel hybrid power system," *IEEE Trans. Energy Convers.*, vol. 26, no. 2, pp. 559–571, Jun. 2011.

[17] N. Kakimoto, S. Takayama, H. Satoh, and K. Nakamura, "Power modulation of photovoltaic generator for frequency control of power system," *IEEE Trans. Energy Convers.*, vol. 24, no. 4, pp. 943–949, Dec. 2009.

[18] S. Eftekharnejad, V. Vittal, G. Heydt, B. Keel, and J. Loehr, "Impact of increased penetration of photovoltaic generation on power systems," *IEEE Trans. Power Syst.*, vol. 28, no. 2, pp. 893–901, May 2013.

[19] N. Mohan, T. Undeland, and W. Robbins, *Power Electronics: Converters, Applications and Design*, 3rd ed. New York, NY, USA: Wiley, 2003.

[20] S. Cole and B. Haut, "Robust modeling against model-solver interactions for high-fidelity simulation of VSC HVDC systems in EUROSTAG," *IEEE Trans. Power Syst.*, vol. 28, no. 3, pp. 2632–2638, Aug. 2013.

[21] S. Rosado, R. Burgos, S. Ahmed, F. Wang, and D. Boroyevich, "Modeling of power electronics for simulation based analysis of power systems," in *Proc. Summer Comput. Simul. Conf.*, 2007, pp. 19–26.

[22] B. K. Johnson, "HVDC models used in stability studies," *IEEE Trans. Power Del.*, vol. 4, no. 2, pp. 1153–1163, Apr. 1989.

[23] K. Clark, R. Walling, and N. Miller, "Solar photovoltaic (PV) plant models in PSLF," in *Proc. IEEE Power & Energy Soc. General Meeting*, Jul. 2011, pp. 1–5.

[24] N. W. Miller, W. W. Price, and J. J. Sanchez-Gasca, "Dynamic modeling of GE 1.5 and 3.6 wind turbine-generators," GE Power Systems, Tech. Rep. 3.0, Oct. 2003.

[25] "Technical update - wind and solar pv modeling and model validation," EPRI, Palo Alto, CA, USA, Tech. Rep. 1025475, 2012.

[26] "PLECS," Plexim Electrical Engineering Software, http://www.plexim.com/home

[27] S. Yang, Q. Lei, F. Peng, and Z. Qian, "A robust control scheme for grid-connected voltage-source inverters," *IEEE Trans. Ind. Electron.*, vol. 58, no. 1, pp. 202–212, Jan. 2011.

[28] PSLF. GE Energy Consulting [Online]. Available: http://www.geenergyconsulting.com/practice-area/software-products/pslf

[29] P. Anderson and A. Fouad, *Power System Control and Stability*, 2nd ed. Piscataway, NJ, USA: IEEE Press, 2003.

[30] N. W. Miller, M. Shao, S. Pajic, and R. D'Aquila, "Western wind and solar integration study phase 3 - frequency response and transient stability," NREL, Golden, CO, USA, Tech. Rep. NREL Report No. SR-5D00-62906, Dec. 2014.

Deepak Ramasubramanian (S'10) received the B.E. degree from the PES Institute of Technology, Bangalore, KA, India, in 2011, and the M.Tech. degree from the Indian Institute of Technology Delhi, New Delhi, India, in 2013. He is currently working toward the Ph.D. degree at Arizona State University, Tempe, AZ, USA.

Ziwei Yu received the B.E. degree from the North China University of Technology, Beijing, China, in 2010, and the M.S. degree from the Arizona State University, Tempe, AZ, USA in 2012, both in electrical engineering. He is currently working toward the Ph.D. degree at Arizona State University, Tempe, AZ, USA.

Rajapandian Ayyanar (M'00–SM'06) received the M.S. degree from the Indian Institute of Science, Bangalore, India, and the Ph.D. degree from the University of Minnesota, Minneapolis, MN, USA. He is currently an Associate Professor in the School of Electrical, Computer and Energy Engineering at Arizona State University, Tempe, AZ, USA.

Vijay Vittal (SM'78–F'97) received the B.E. degree from the B.M.S. College of Engineering, Bangalore, KA, India, in 1977, the M.Tech. degree from the Indian Institute of Technology, Kanpur, Kanpur, UP, India, in 1979, and the Ph.D. degree from Iowa State University, Ames, IA, USA, in 1982, all in electrical engineering.

He is the Ira A. Fulton Chair Professor in the Department of Electrical, Computer, and Energy Engineering at Arizona State University, Tempe, AZ, USA. He currently is the Director of the Power System Engineering Research Center (PSERC).

Dr. Vittal is a member of the National Academy of Engineering.

John Undrill (F'78) received the Ph.D. degree from the University of Canterbury, Christchurch, New Zealand. He is currently a Research Professor at Arizona State University, Tempe, AZ, USA.